Effects of Alloying Elements (Ti and *x*Al) on the Electrochemical Corrosion Behaviour of Iron-Based Alloys in Corrosive Solutions of Different pH

Mohamed M. El-Rabiei[1] · **Ghada M. Abd El-Hafez**[1] · **Amira H. Ali**[1]

Abstract

In this research, the effects of Ti addition, increased Al content ($x = 12$, 19 and 28 wt%) and pH of the corrosive solution on the corrosion behaviour of Fe, Fe–12Al, Fe–19Al, Fe–28Al and Fe–7.7Al–8.5Ti alloys were electrochemically studied through the potentiodynamic polarization (PDP), open-circuit potential (OCP) and electrochemical impedance spectroscopy (EIS) measurements. In all test solutions, the OCP reported generally that the open-circuit potential shift is positive compared to the Fe-alloy. The PDP results confirmed that the investigated alloys record a decrease in the corrosion rate in the following order: Fe–7.7Al–8.5Ti < Fe–*x*Al < Fe. Also, the corrosion current density (i_{corr}) decreases with increasing the Al content. The experimental impedance data clearly confirmed that, increased Al content in the binary Fe–*x*Al alloys increases the corrosion resistance; moreover, ternary Fe–Al–Ti was superior to Fe–*x*Al against corrosion where more thicker and resistant passive layer is formed on the Fe–Al–Ti alloy surface. For all alloys, the corrosion resistance reaches maximum passivation in neutral rather than acidic or basic solution. The charge-transfer resistance, R_{ct}, was compared with the polarization resistance, R_p, for accurate analysis of the EIS and PDP results. The surface analysis (SEM/EDAX) showed the participation of the different alloying elements in the protection according to the alloy constituents. It turned out that presence of Al and Ti increase the corrosion resistance. For industrial applications, the results lead to the recommendation of the Fe–7.7Al–8.5Ti alloy in the industrial chemical processes which require high corrosion resistance as that of halides resistance.

1 Introduction

Iron-based alloys can be applied in wide fields due to their excellent properties [1]. The development of some iron-based alloys such as Fe–Al and Fe–Ti alloys has a major concern related to their properties and their performances compared to steel's constituent pure elements, namely, iron, aluminium and titanium. Indeed, there are some industrial and economic reasons, such as the reduction of material density and costs or environmental nuisances, explain why these materials are highly sought by certain industries, in particular, aeronautics industries. Today, they are used for

properties such as hardness, friction resistance, corrosion resistance and high-temperature [2–7]. As a result, Fe–Ti alloys are good resistant materials to friction and are widely used in the automotive industry. The Ti–Al intermetallic materials are potential alloys for the chemical, energy and aerospace industries [2]. The Fe–Al iron-based alloys are important structural intermetallics due to their remarkable corrosion resistance, even in aggressive environments, low density, low cost, good mechanical properties and environmental friendliness [2, 6]. These materials have a very limited commercialization due to their inadequate creep strength at elevated temperatures and impact resistance at ambient temperature, therefore these intermetallics have been developed mainly at elevated temperatures for structural applications; many studies have also focused on the corrosion behaviour of Fe–Al alloys so far, but they mainly focused on binary Fe–Al alloys with a limited variation of the Al content or with additional alloying elements [8–11].

✉ Amira H. Ali
  ah1173@fayoum.edu.eg

1 Chemistry Department, Faculty of Science, Fayoum University, Fayoum, Egypt

Recent studies [12–17] have discussed the influence of some alloying elements addition to overcome some barriers that limit the wide usage of the binary Fe–Al alloys such as their low ductility at room temperatures. Previous researchers have reported that alloying elements have an influence on the corrosion performance of the binary Fe–Al alloys in different corrosion media, but the electrochemical behaviour is sparse in all of these studies [18–24]. The results of these studies suggest that iron aluminides may contribute in certain biomedical applications and in a number of land-based applications such as marine, chemical and petrochemical industries [13, 17]. Despite the potentials of titanium containing alloys, the high cost of the alloys has limited their use to applications where they are the only choice that satisfies the intended service requirements [25]. The highly priced titanium and its alloys were developed by partially substituting some expensive alloying elements such as vanadium with iron in order to reduce the cost of stabilizing the β phase [14]. However, TiFe has been reported to have deleterious effect on the mechanical and corrosion properties of titanium containing alloys [25].

Moreover, the corrosion of iron aluminide alloys has been reported in different aggressive solution; it has been found that, the breakdown of the protective layer of iron occurs in the presence of Cl^- and SO_4^{2-} ions [26–28]. Masahashi et al. [29] tested the Fe–Al alloys in 5×10^{-3} M H_2SO_4 with a wider range of Al content (5, 10, 15, 25 and 30 at.%). However, only the mass change of the samples was determined after immersion in the test solution and the passivation behaviour was not investigated. A more extensive study was done by Chiang et al. [30] who studied the passivation behaviour of six Fe–Al alloys in sulfuric acid solution with Al contents between 3.4 and 41.7 at.% at 25 °C. However, no post mortem examinations were performed. A summarized study [11] was carried out on the compositions of the binary Fe–Al alloys and electrolytes investigated in different investigations. In summary, it has been recently concluded that a systematic study of the aqueous corrosion behaviour of binary Fe–Al alloys is still necessary [8].

The present work has a main objective of comparing the electrochemical corrosion behaviour of binary Fe–xAl and ternary Fe–Al–Ti iron-based alloys in corrosive solutions of different pH. The aim was focused on studying the effects of Ti and xAl as alloying elements on the corrosion passivation of iron-based alloys at pH 2, 7 and 12. The study was carried out using potentiodynamic polarization (PDP), open-circuit potential (OCP) and electrochemical impedance spectroscopy (EIS) measurements, as well as energy-dispersive X-ray (EDAX) spectroscopy and scanning electron microscopy (SEM). Fitting of the experimental impedance data to theoretical values according to equivalent circuit models enables understanding of the corrosion mechanism and explains the electrochemical behaviour of the alloy/solution interface.

2 Experimental

A three-electrode all-glass double-jacket cell was used in the electrochemical measurements, including an auxiliary platinum counter electrode with an area of 1.0 cm^2 and the Fe-alloys that served as working electrodes with a connection area of 0.5 cm^2 in addition to a saturated reference calomel electrode (SCE). The working electrode was placed in the centre of the cell in such a manner that the electrode was adjacent to the platinum counter electrode and the reference electrode, as presented in Fig. 1. The double-jacket cell was connected to constant–temperature water circulators. An ultrathermostat (BT-22 model, Spain) was used. The working electrodes consisted of massive rods with diameters corresponding to circular surface areas of 0.5 cm^2 for Fe and its alloys. These electrodes were mounted in suitable glass tubes using a two-epoxy component. The investigated electrodes were commercial-grade rods of Fe, Fe–xAl (where x denotes the Al percentage), and Fe–Al–Ti; the spectrometric mass analysis of the alloys utilized in the electrodes is shown in Table 1. For all measurements carried out in this work, each experiment proceeded as follows: the Fe-alloys were washed with triple-distilled water, subjected to mechanical polishing through different emery papers graded from 500 to 2500, then thoroughly rubbed with a very smooth polishing cloth and quickly transferred to the cell. In particular, all measurements were carried out at pH 2 (54.3 ml 0.1 M HCl + 44.2 ml 0.1 M potassium biphthalate ($C_8H_5KO_4$) + 151.5 ml H_2O), pH 7 (56.8 ml 0.2 M NaOH + 113.6 ml 0.2 M KH_2PO_4 + 79.6 ml H_2O), and pH
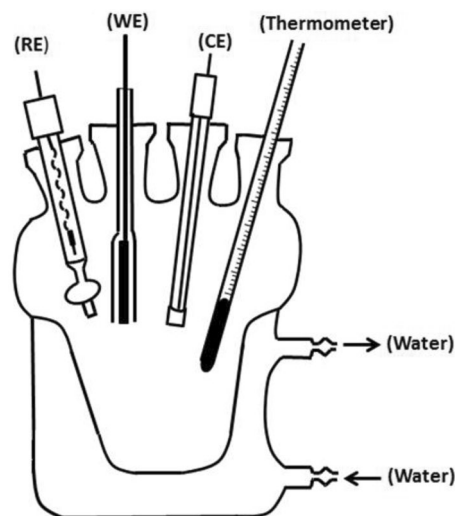

Fig. 1 The electrochemical working cell

Table 1 Composition of the investigated alloys (wt%) determined by mass spectrometry

Alloy	Al%	Ti%	C%	Ni%	S%	Cr%	P%	Fe%
Fe	0.01	–	0.34	0.02	0.02	0.01	0.04	Remainder
Fe–12.3Al	12.3	0.0025	0.422	0.037	0.027	0.011	0.034	Remainder
Fe–19.7Al	19.7	0.0043	0.476	0.035	0.024	0.014	0.035	Remainder
Fe–28.6Al	28.6	0.0056	0.482	0.020	0.022	0.011	0.029	Remainder
Fe–7.7Al–8.5Ti	7.7	8.5	0.273	0.043	0.046	0.018	0.044	Remainder

12 (163.7 ml 0.2 M NaOH + 100 ml 0.2 M KH$_2$PO$_4$). All aqueous buffer solutions were prepared using analytical-grade reagents and triple-distilled water (Sigma Aldrich). Each experiment was preceded by evaluation for the pH of the prepared solution by a standard BT-500 model pH meter (Germany).

PDP and EIS experiments were conducted all-in-one potentiostat/galvanostat using a Voltalab 10 PGZ 100 (France) controlled by Volta master 4 Tacussel software for corrosion analysis. The instrument was connected to an external IBM 1200 CPU computer. All measured potentials were recorded at room temperature against the standard potential of the SCE ($E^0 = 0.245$ V vs. SHE). The electrode was kept in the test solution until the steady-state potential, E_{ss}, varied by less than 0.1 mV min^{-1}. A scan rate of 10 mV s^{-1} was applied in all Polarization measurements. The polarization data were extrapolated to determine the corrosion parameters, i.e. current density (i_{corr}), corrosion potential (E_{corr}), corrosion rate, and Tafel slopes (β_a and β_c). Electrochemical impedance (Z) measurement was conducted at a frequency range from 0.1 to 10^5 Hz. In all EIS experiments, the superimposed AC signal had a 10 mV peak-to-peak amplitude. Each experiment was performed at least twice to obtain the statistical accuracy of the results. The surface morphology and the content of different elements were inspected by SEM and EDAX measurements, respectively, before and after electrode examination in the different corrosive solutions. SEM analysis of the investigated samples was performed using a Quanta 250 FEG (field emission gun) microscope coupled with an EDAX unit using a resolution of 1 nm, a magnification from ×14 to ×1,000,000, and an accelerating voltage of 30 kV.

3 Results and Discussion

3.1 OCP Measurements

The OCP measurements of the Fe, Fe–xAl, and Fe–Al–Ti alloys against SCE were recorded and tested for 60 min in stagnant buffer of pH 2, 7, and 12 at 25 °C using a high impedance auto-ranging multimeter (Keithley Model 130A, Germany) to record the individual test potentials. In the case of the iron alloy without added alloying elements, the E_{ss}

values were shifted to less positive potentials than those of binary and ternary alloys. This shift is related to the continuous dissolution of the iron sample in the test solution due to the non-protective nature of its native surface film. The addition of Ti and xAl alloying elements to the iron alloy shifted the OCP to a more positive value, indicating that the active sites at the surface were blocked, and thus, the corrosion rate was decreased. The value of E_{ss} was always more positive than the immersion value (E_{oc} at $t = 0$), suggesting that the film formed before immersion caused additional dissolution. This result interpreted that the anodic rate reaction was decreased rather than the cathodic reaction. For all alloys, the OCP was found to reach a steady-state value within 30–40 min after electrode immersion in acidic and basic solutions; however, in neutral electrolytes, steady state was reached 10 min after immersion, as shown in Fig. 2. These results indicated that the alloys generally tended to initially passivate, followed by corrosion of the passivation film in acidic or basic electrolyte solutions, where more corrosion and passivation processes occur at the electrode surface, whereas the surface was rapidly stabilized in neutral solution. Moreover, the Ti addition to Fe–Al alloy increased E_{ss} in all three aqueous media compared to those of Fe–xAl alloys, as shown in Table 2, and we explored this hypothesis further using potentiodynamic and impedance measurements, as described in Sects. 3.2 and 3.3.

3.2 PDP Measurements

The PDP measurements of Fe, Fe–xAl, and Fe–Al–Ti electrodes in stagnant buffer of pH 2, 7, and 12 at 25 °C were investigated. The PDP results were recorded after the electrode had reached E_{ss}. The data obtained are presented in Fig. 3, which shows the PDP curves for the working alloys. All polarization curves for the binary and ternary iron-based alloys were qualitatively similar and generally showed a decrease in the corrosion current density, i_{corr}, as Ti and xAl alloying elements were added to the iron-based alloy. The Tafel extrapolation method applied to analyse the polarization curves and calculate the corrosion parameters, i.e. E_{corr}, i_{corr}, polarization resistance (R_p), β_a, and β_c, reported in Table 3. This table shows that, the addition of Ti and (x)Al increased the corrosion resistance of the Fe-based alloys in all different solutions. In particular, an increase of Al content

Fig. 2 Time dependence of the open-circuit potential of Fe, Fe–xAl, and Fe–Al–Ti electrodes. **a** pH 2, **b** pH 7, **c** pH 12
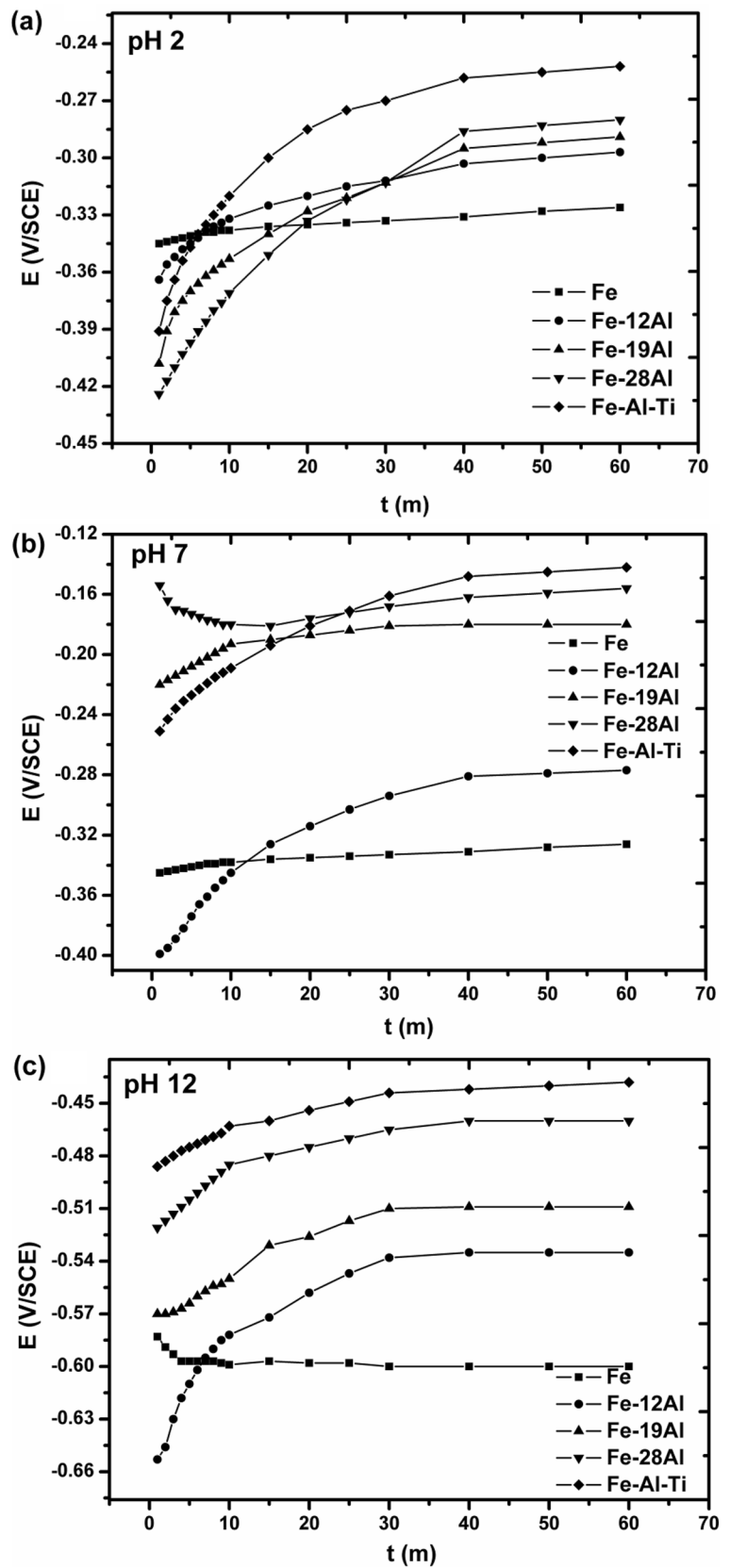
Table 2 Steady-state potentials measured for Fe, Fe–xAl, and Fe–Al–Ti alloys at 25 °C and pH 2, 7, and 12

Alloy	E_{ss} (V/SCE)		
	pH 2	pH 7	pH 12
Fe	− 0.326	− 0.326	− 0.6
Fe–12Al	− 0.297	− 0.277	− 0.535
Fe–19Al	− 0.289	− 0.18	− 0.509
Fe–28Al	− 0.28	− 0.156	− 0.46
Fe–Al–Ti	− 0.252	− 0.142	− 0.438

in the binary Fe–xAl alloys increased the corrosion resistance; moreover, the addition of Ti to the Fe–Al alloy (forming Fe–7.7Al–8.5Ti) resulted in the lowest corrosion rate in all aqueous media, as shown in Fig. 4, indicating that the corrosion rate of the investigated materials in basic, acidic, and neutral solutions decreases in the following order: Fe > Fe–12.3Al > Fe–19.7Al > Fe–28.6Al > Fe–7.7Al–8.5Ti. This observation can be explained by considering that the growth of a protective Al_2O_3 layer was enhanced on the iron alloys by the addition of Al; the formation of this layer on the alloy reduces the corrosion rate [31]. The external Al_2O_3 domain was always observed for alloys with Al contents between 2.4 and 6.9 wt%, but this domain was penetrated with iron oxide nodules that interspersed the alloy substrate and whose formation was suppressed only once the aluminium content exceeded approximately 7 wt% [32]. In addition, the critical Al content for the formation of Al_2O_3 on the alloy has been found to increase with the addition of titanium [32], which may explain the lowest corrosion rates of the Fe–Al–Ti system among the alloys investigated in this study.

The investigated materials also showed lower corrosion rates in neutral than acidic and basic media (Fig. 4). This difference can be explained based on thermodynamic considerations. Al-containing alloys are nominally passive at pH 7 as a result of a protective Al_2O_3 film formation. However, under acidic and basic conditions, this protective film becomes soluble, and its continuity is disrupted, resulting in the dissolution of the alloy surface. In acidic conditions, Al is oxidized to Al^{3+}, whereas in the alkaline conditions, AlO_2^{2-} ions are formed [33, 34], this can be clear from the Pourbaix diagram in Fig. 5 [35].

3.3 EIS measurements

Steady-state EIS can be used to confirm the results of corrosion rate measurements performed by conventional polarization techniques. Both Bode and Nyquist diagrams can be used to display and analyse the EIS data; these plots are shown in Figs. 6 and 7, respectively. All impedance data in the whole frequency domain are explicitly represented in the standard Bode plots. Nyquist plots illustrate the difference

between the R_p values of the investigated alloys in various solutions [36].

The open-circuit impedance of the Fe, Fe–xAl, and Fe–Al–Ti alloys was recorded over 60 min following electrode immersion in the acidic, basic, or neutral test solutions. At low frequencies, the Bode diagrams of the data obtained in acidic, neutral, and basic solutions (Fig. 6a, b, and c, respectively) display a single phase maximum, indicating that the corrosion process was controlled by one time constant. In these plots, the maximum phase angle of the investigated materials decreases in the following order: Fe–7.7Al–8.5Ti > Fe–28.6Al > Fe–19.7Al > Fe–12.3Al > Fe; this trend reflects the higher R_p values measured for the Fe–Al–Ti alloy than for Fe and Fe–xAl. In addition, increased Al content in the binary Fe–xAl alloys increases the R_p values.

The Nyquist plots of the working materials in acidic, neutral, and basic solutions (Fig. 7a, b, and c, respectively) are similar to each other, except for the diameters of the semicircles denoting R_p; this relationship indicates that these materials have different R_p values despite their similar corrosion mechanism [37]. In these plots, the addition of Ti and xAl alloying elements to the Fe matrix increases the R_p of the metallic material in the Fe matrix; this increase can be confirmed by tracking the diameters of the semicircles of the investigated materials. The diameters decrease in the following order: Fe–7.7Al–8.5Ti > Fe–28.6Al > Fe–19.7Al > Fe–12.3Al > Fe; this trend reflects the higher R_p measured for the Fe–Al–Ti alloy than for Fe and Fe–xAl, which also confirmed the Bode results.

For all alloys, passivation phenomena were more clearly observed in neutral than in acidic and basic solutions. In order to clarify the corrosion behaviour of the working alloys at different pH values, the same data reported in Figs. 6 and 7 are partially reproduced in an illustrative example in Fig. 8a and b. This example shows the impedance Bode and Nyquist plots, respectively, for the Fe–28Al electrode in stagnant buffer of pH 2, 7, and 12. All alloys behaved similarly to the Fe–28Al alloy at different pH values. From Fig. 8a and b, the maximum phase angle and semicircle diameter, respectively, decrease in the following order: pH 7 > pH 2 > pH 12. This trend confirms that neutral solution possesses higher R_p than basic and acidic solutions. This pH dependence is clear from the appearance of diffusion-controlled processes in neutral solution only; the presence of such processes was detected in the Nyquist diagram (Fig. 8b) as a linear region at the low-frequency part [38].

An accurate analysis of impedance data was carried out using equivalent circuit models. The EIS data for the working electrodes were fitted to the two circuits shown in Fig. 9a and b. Model (a) fits the data obtained in acidic and basic solutions, while model (b) corresponds to neutral solution. The model presented in Fig. 9a consisted of a charge-transfer (corrosion) resistor (R_{ct}) and a double-layer capacitor (C_{dl})

Fig. 3 Potentiodynamic polarization curves of Fe, Fe–*x*Al, and Fe–Al–Ti electrodes. **a** pH 2, **b** pH 7, **c** pH 12
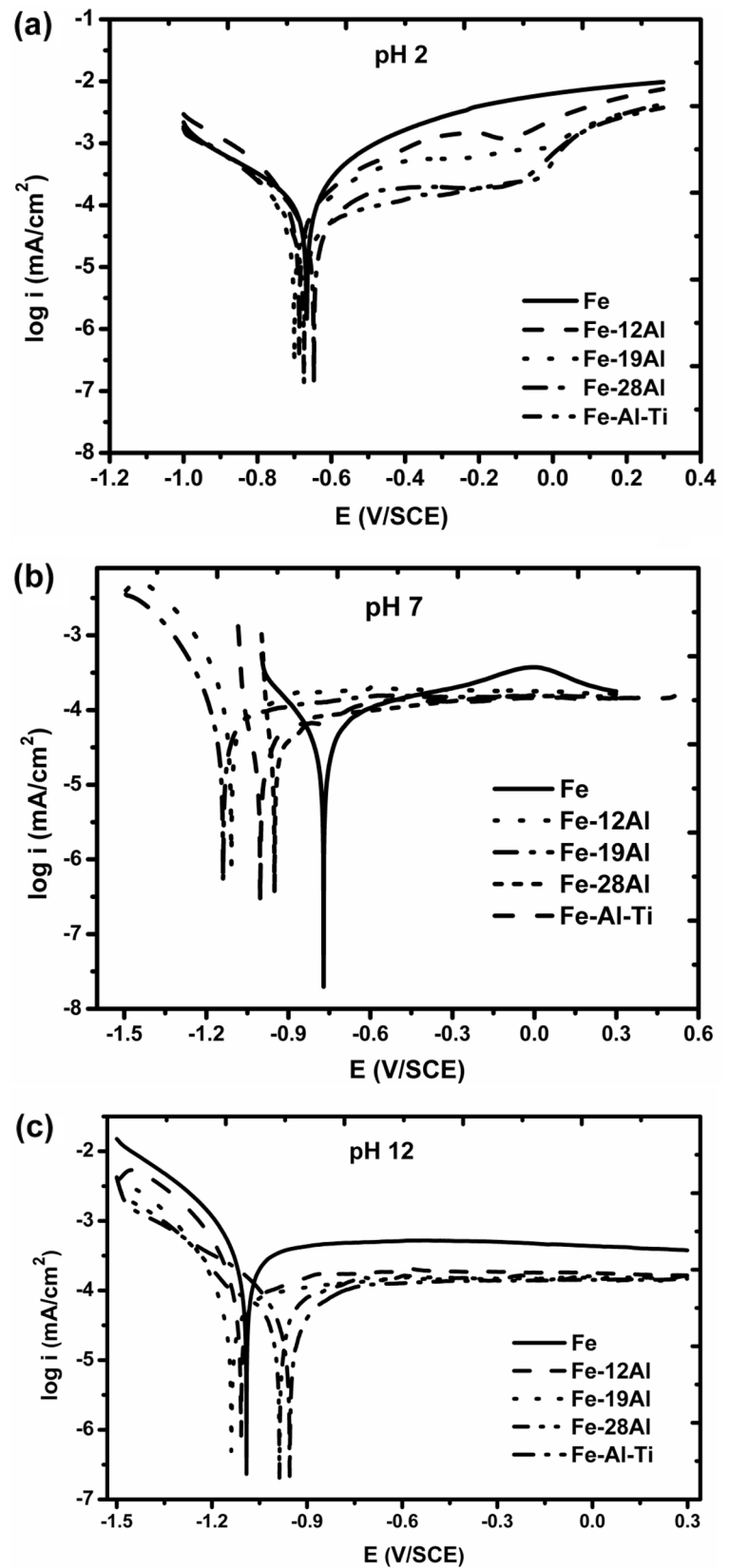
Table 3 Polarization parameters and corrosion rates of Fe, Fe–xAl, and Fe–Al–Ti electrodes at 25 °C and pH 2, 7, and 12

pH	Alloys	E_{corr} (V)	R_p (Ω cm^2)	i_{corr} (mA/cm^2)	β_a (mV)	β_c (mV)	Corrosion rate (mm/year)	η (%)
2	Fe	− 0.666	316.36	0.069	117.0	− 178.6	802.9	–
	Fe–12.3Al	− 0.713	371.21	0.064	138.1	− 143.2	746.4	7.2
	Fe–19.7Al	− 0.684	414.54	0.055	168.2	− 111.3	640.7	20.3
	Fe–28.6Al	− 0.7	600.96	0.045	177.8	− 127.2	524.6	34.8
	Fe–7.7Al–8.5Ti	− 0.647	801.1	0.032	178.4	− 131.7	373.8	53.6
7	Fe	− 0.771	1040	0.026	204.9	− 167.0	298.9	–
	Fe–12.3Al	− 0.984	1130	0.025	162.9	− 181.5	289.0	3.8
	Fe–19.7Al	− 0.954	1160	0.02	185.2	− 130.0	239.4	23.1
	Fe–28.6Al	− 0.862	1340	0.017	176.4	− 108.7	203.4	34.6
	Fe–7.7Al–8.5Ti	− 0.92	1420	0.009	86.4	− 64.6	105.8	65.4
12	Fe	− 1.09	181.02	0.158	270.5	− 126.6	1848	–
	Fe–12.3Al	− 1.107	362.88	0.093	67.8	− 118.6	1086	41.1
	Fe–19.7Al	− 1.108	400.27	0.084	400.7	− 111.4	981.3	46.8
	Fe–28.6Al	− 1.112	413.75	0.078	468.8	− 110.1	912.6	50.6
	Fe–7.7Al–8.5Ti	− 1.138	677.79	0.04	259.2	− 107.8	462.4	74.7
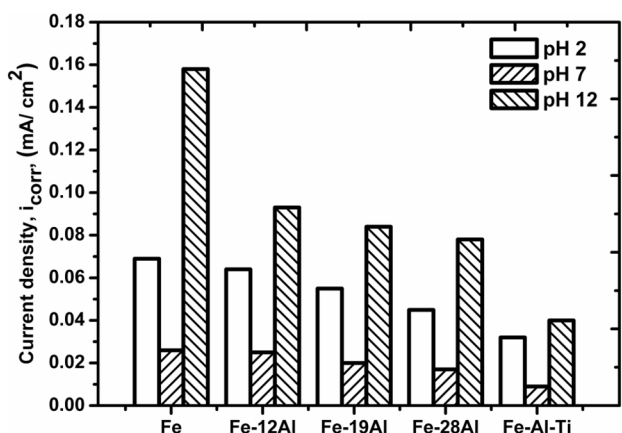
Fig. 4 Corrosion rates of Fe, Fe–xAl and Fe–Al–Ti in test solutions with different pH values

Fig. 5 Pourbaix diagram for aluminium at 25 °C

connected in parallel with each other and in series with a solution resistor (R_s). In addition, the corrosion rate is proportional to $1/R_{ct}$. In this case, the impedance, Z, is given by the following equation [39]:

$$Z = R_s + [R_{ct}/(1 + (2\pi f R_{ct} C_{dl})\alpha)] \qquad (1)$$

where f is the frequency in Hz and α is an empirical parameter ($0 \leq \alpha \leq 1$). This relation accounts for the deviations from the ideal capacitor (R_C) behaviour associated with time constant distributions due to surface inhomogeneity, roughness, and variations of surface layer properties [39]. In neutral solutions (Fig. 7b), a Randles equivalent circuit (Fig. 9b) with a constant-phase element (CPE) was introduced to

analyse the impedance date arising from a linear range of experimental system corresponding to a simple charge-transfer process, as proposed by Brug et al. [40].

The impedance parameters of the investigated alloys were calculated and presented in Table 4. The table highlights an inverse relationship between R_{ct} and the corrosion rate, implying that the addition of Ti and (x)Al alloying elements to the iron-based alloys decreases the corrosion rate (increases the polarization resistance); in particular, at all pH values, the highest and lowest R_{ct} values were obtained for Fe–7.7Al–8.5Ti and Fe, respectively. In addition, an R_{ct} increase was accompanied by a decrease in C_{dl} only in neutral solution, confirming that the investigated alloys can form

Fig. 6 Bode plots of Fe, Fe–
*x*Al, and Fe–Al–Ti electrodes. **a**
pH 2, **b** pH 7, **c** pH 12
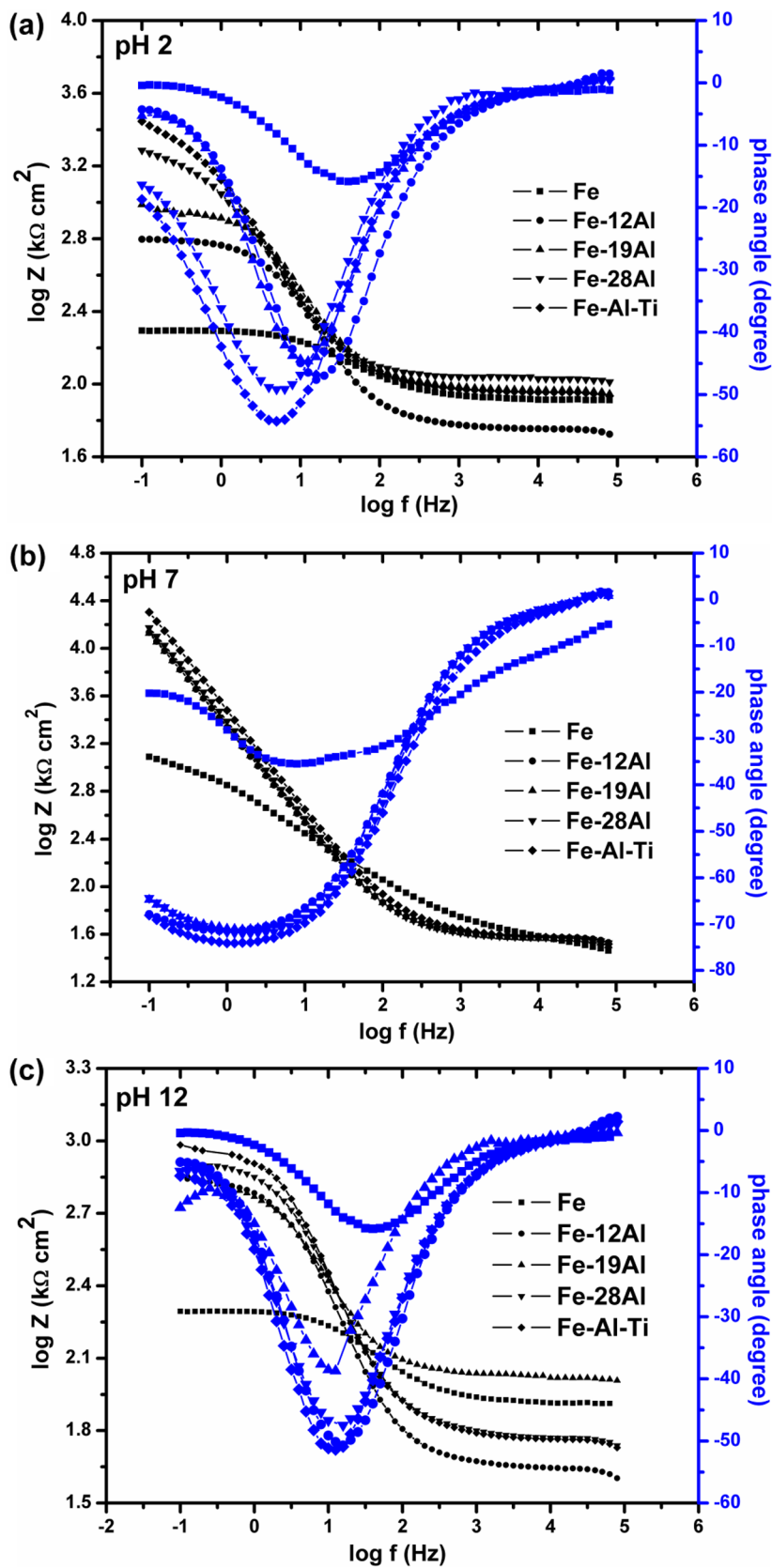
Fig. 7 Nyquist plots of Fe, Fe–*x*Al, and Fe–Al–Ti electrodes. **a** pH 2, **b** pH 7, **c** pH 12
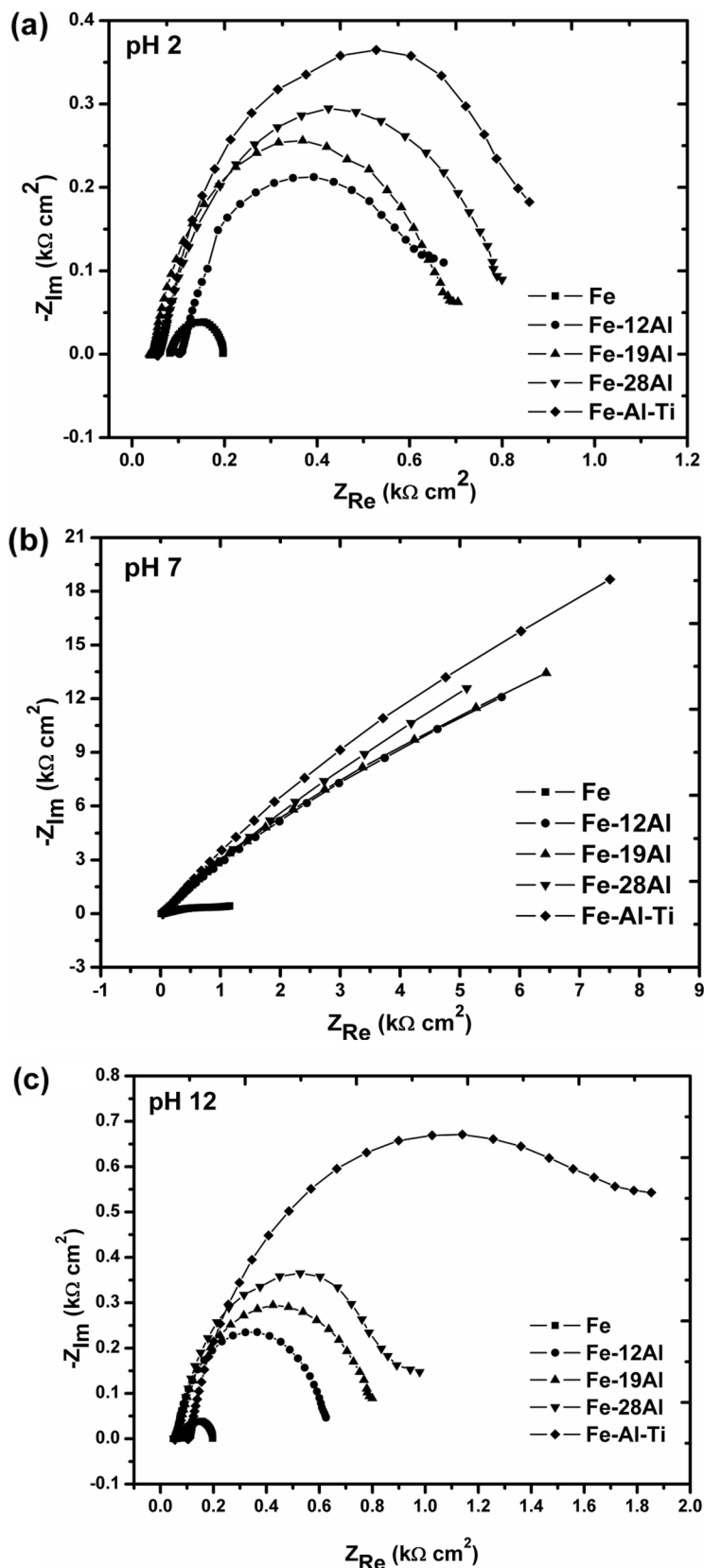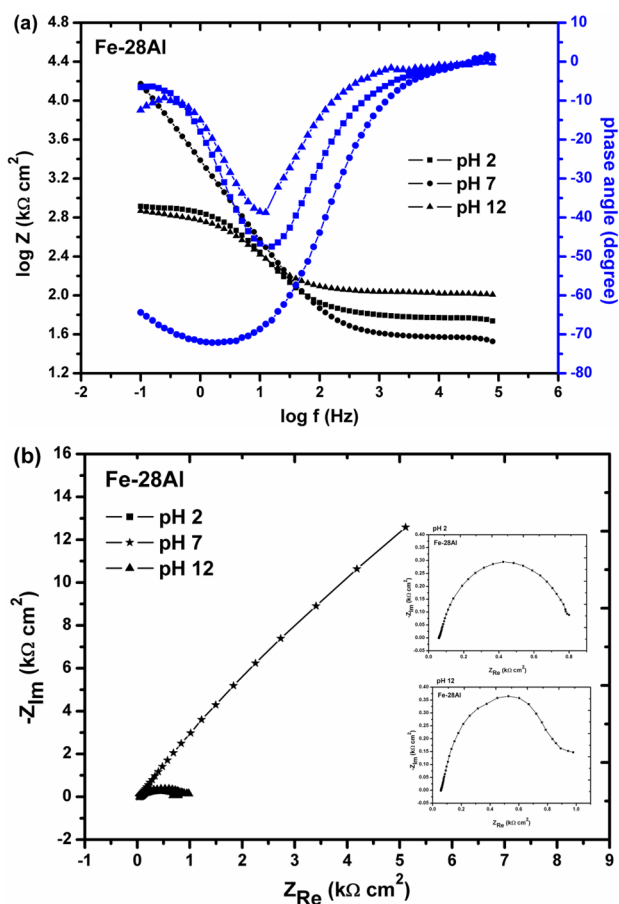
Fig. 8 Bode (**a**) and Nyquist (**b**) plots of the Fe–28Al alloy at pH 2, 7, and 12

a stable protective film in neutral solution, in contrast to those formed in acidic and basic solutions. A similar observation was recorded upon (x)Al addition to Mg–Al alloy [41].

Figure 10 showed a qualitative comparison between the values of the R_p and R_{ct} for the different techniques: PDP and

EIS, respectively, in acidic solution (an illustrative example and all alloys behaved similarly in other solutions). As can be seen in the figure, the trend for both parameters is practically the same, i.e. the highest values for these parameters measured for the Fe–Al–Ti alloy. Although the two techniques had a similar trend, they presented different values, i.e. the highest value on this figure was estimated by the EIS technique. In this work, we consider that the electrochemical technique that better describes the corrosion of iron immersed in different solutions is that which takes into account the ohmic drop. For this reason, the EIS gives a good approximation to the real corrosion rates for the proposed system. A similar behaviour for the corrosion of iron immersed in Na_2SO_4 solutions can be observed in Ref. 42.

3.4 Surface Morphology

To identify the distribution and nature of microstructures that influence corrosion behaviour, a microstructural study was conducted on the different specimens. A scanning electron microscope attached to an EDAX unit was used to characterize the microstructures of the different polished or corroded surfaces. The SEM images in Fig. 11a–d show the smooth surfaces of mechanically polished Fe, Fe–12Al, Fe–28Al, and Fe–Al–Ti alloys, respectively, before immersion in the investigated solution, which reflects the decrease in corrosion rate and surface passivation.

The corrosion sites and flawed regions were investigated by performing SEM and EDAX measurements after 60 min immersion of the samples in a neutral aerated solution at 25 °C. The SEM and EDAX images of the Fe, Fe–12Al, Fe–28Al, and Fe–Al–Ti alloys are shown in Fig. 12a–d, respectively. The SEM images of all alloys show a decrease in the surficial roughness in the following order: Fe–7.7Al–8.5Ti < Fe–28.6Al < Fe–12.3Al < Fe; this trend reflects that, upon alloying with Al and Ti, the corrosion pitting decreased [43]. Accordingly, Fe exhibited the greatest corrosion pitting among all samples. An
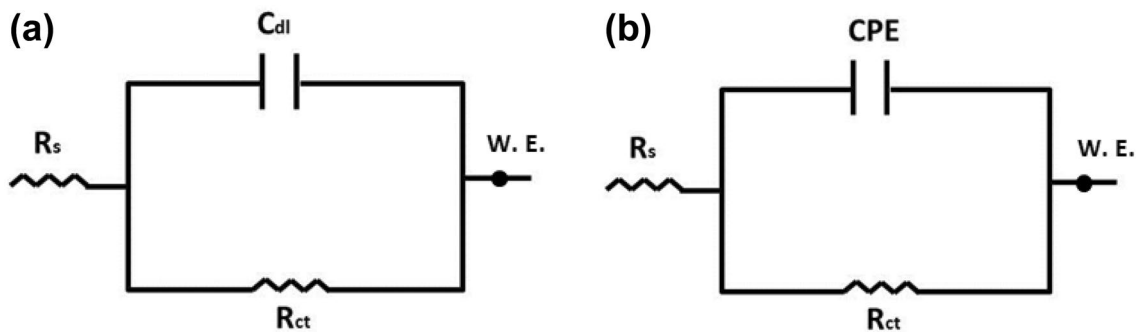

Fig. 9 Equivalent circuit models of the experimental impedance data of Fe, Fe–xAl, and Fe–Al–Ti. Model (**a**) fits the data obtained in acidic and basic solutions, while model (**b**) corresponds to neutral solution

Table 4 Equivalent circuit parameters (Eq. 1) of the impedance data in acidic, basic and neutral solutions, measured for Fe, Fe–xAl, and Fe–Al–Ti electrodes after immersion in test solutions at 25 °C

pH	Sample	R_S (kΩ cm^2)	R_{ct} (kΩ cm^2)	C_{dl} (µF/cm^2)	α
2	Fe	0.06171	0.5619	56.64	1
	Fe–12.3Al	0.02442	0.6781	74.16	1
	Fe–19.7Al	0.1209	0.7535	168.9	1
	Fe–28.6Al	0.06174	0.8724	57.64	1
	Fe–7.7Al–8.5Ti	0.07912	1.992	100.6	0.999
7	Fe	0.03024	1.901	418.5	0.993
	Fe–12.3Al	0.033	89.90	17.70	1
	Fe–19.7Al	0.03488	92.41	17.22	1
	Fe–28.6Al	0.03958	147.5	10.78	1
	Fe–7.7Al–8.5Ti	0.03717	149.2	10.66	1
12	Fe	0.09243	0.1058	75.20	0.99
	Fe–12.3Al	0.09731	0.502	50.09	1
	Fe–19.7Al	0.009746	0.6904	72.83	1
	Fe–28.6Al	0.06872	0.7383	68.11	1
	Fe–7.7Al–8.5Ti	0.1039	0.8065	62.35	1
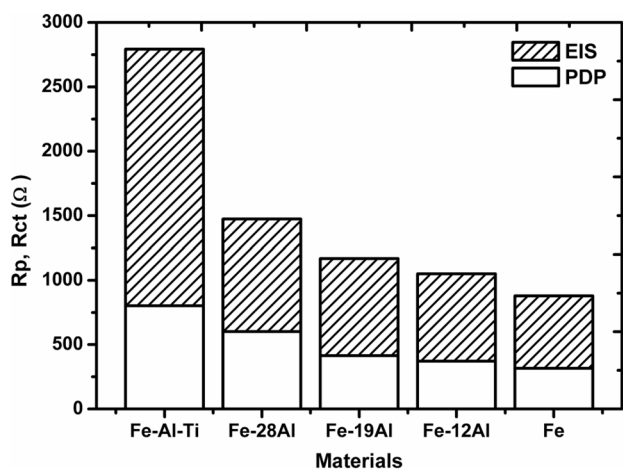
Fig. 10 Qualitative comparison between polarization resistance, R_p, and the charge-transfer resistance, R_{ct}, as a function of different alloying elements in acidic solution of pH 2

increase in Al content resulted in reduced corrosion pitting on the surface of the binary Fe–xAl alloys, but this increase was less effective than that for the ternary Fe–Al–Ti alloy, which presents the fewest surficial pits, taking into account the SEM micrographs of mechanically polished alloys; this observation was confirmed by the EDAX spectra shown in the same figures. The EDAX data (Fig. 12a–d) reflect the content of different elements on the surfaces of the investigated materials after 1 h immersion in neutral solution at 25 °C; in particular, the oxygen content decreased in the

following order: Fe–7.7Al–8.5Ti < Fe–28.6Al < Fe–12.3Al < Fe, as shown in Table 5. This trend reflects the highest oxygen content (and therefore, the highest surface roughness and corrosion pitting) on the surface of the iron matrix, as shown in Fig. 12a. An increase in Al content led to a gradual decrease in the oxygen content, so a lower corrosion pitting was observed on the surface of the Fe–28Al (Fig. 12c) than the Fe–12Al (Fig. 12b) alloy. The presence of Ti (Fig. 12d) in all test solution resulted in repaired flawed regions, so the Fe–Al–Ti alloy showed the lowest oxygen content, which was consistent with the polarization and impedance data. This difference can be resulted from the formation of the Al$_3$Ti phase upon Al–Ti addition to iron alloy (forming Fe–7.7Al–8.5Ti). A similar observation was recorded upon Ti addition to Al–Si alloys [44], which showed that increasing the volume fraction of the Al$_3$Ti phase resulted in increased microhardness of the binary alloy, so high corrosion resistance was observed [44–46]. In this paper, this behaviour was confirmed for Fe–Al–Ti by electrochemical measurements.

Finally, the effect of the different corrosive media is illustrated in Fig. 13, which shows the SEM images of Fe–Al–Ti (a–c) electrode taken after 60 min from the electrode immersion in the acidic, basic, or neutral test solutions. The pitting and corrosion features of the alloys reflect their lower corrosion resistance in basic (Fig. 13c) and acidic (Fig. 13a) solutions and reveal severe damage due to the pronounced corrosion attack on their surfaces. In contrast, in neutral solutions, a smooth surface appeared as a result of a protective Al$_2$O$_3$ layer formation (Fig. 13b).

4 Conclusion

The electrochemical corrosion behaviour of Fe-based alloys has been developed by the addition of Ti and different contents of xAl (x = 12, 19 and 28 wt%) tested in pH 2, 7 and 12. The interpretation of the results was explained through OCP, PDP and EIS measurements and the resultant passive film formed on the iron surfaces has been investigated by SEM and EDAX analyses. For all alloying elements the following is given:

- The OCP measurements recorded more positive E_{ss} shift compared to the iron alloy.
- The PDP results showed a decrease in the corrosion rate in the following order: Fe–7.7Al–8.5Ti < Fe–28.6Al < Fe–19.7Al < Fe–12.3Al < Fe.
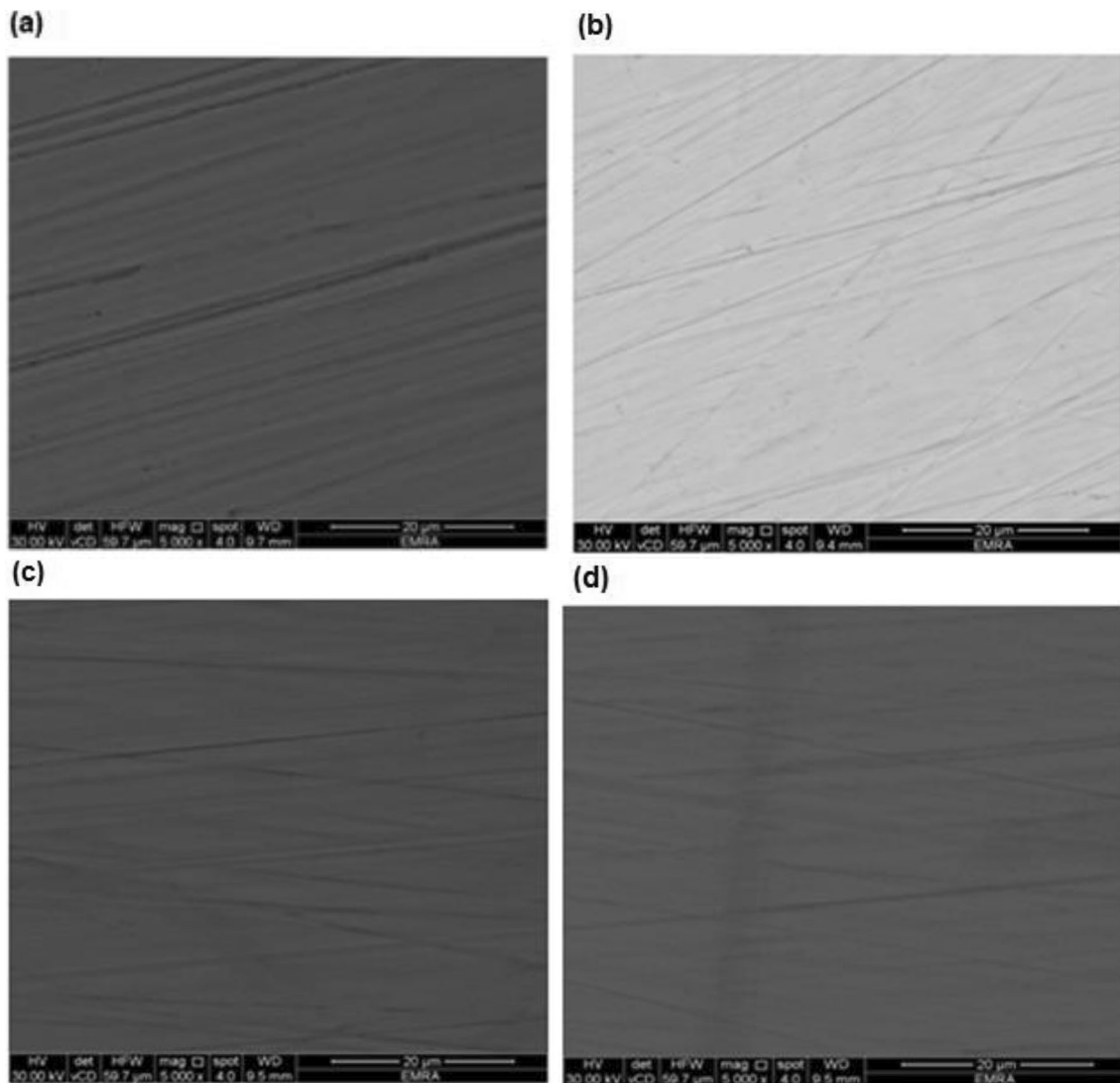
Fig. 11 Scanning electron micrographs of investigated alloys before immersion. **a** Fe; **b** Fe–12Al; **c** Fe–28Al; **d** Fe–Al–Ti

- The EIS data showed more surface and polarization resistance than the iron alloy.
- Neutral solution recorded lower corrosion rates than acidic or basic conditions.
- R_{ct} values determined from EIS followed a behaviour very similar to R_p obtained by PDP. Taking into account the ohmic drop, EIS is the technique that better describes the corrosion of iron in different solutions.
- The SEM and EDAX analyses showed lower corrosion pitting and oxygen content than Fe-alloy.
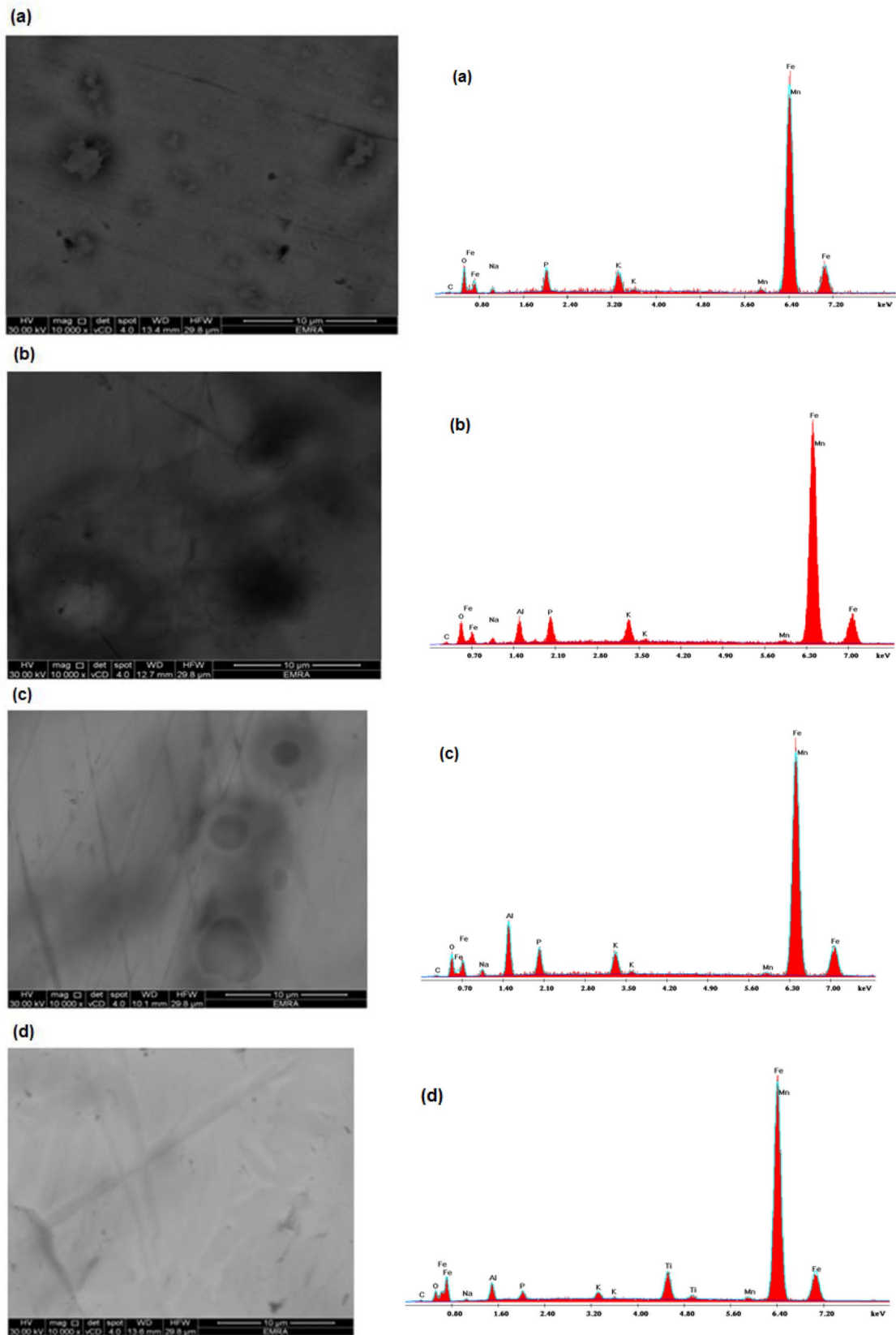
Fig. 12 Scanning electron micrographs and energy-dispersive X-ray spectra of the working electrodes after 1 h immersion at pH 7 and 25 °C. **a** Fe; **b** Fe–12Al; **c** Fe–28Al; **d** Fe–Al–Ti

Table 5 Oxygen content values (wt%) obtained from EDAX analysis for Fe, Fe–12Al, Fe–28Al and Fe–Al–Ti electrodes after 1 h immersion at pH 7 and 25 °C

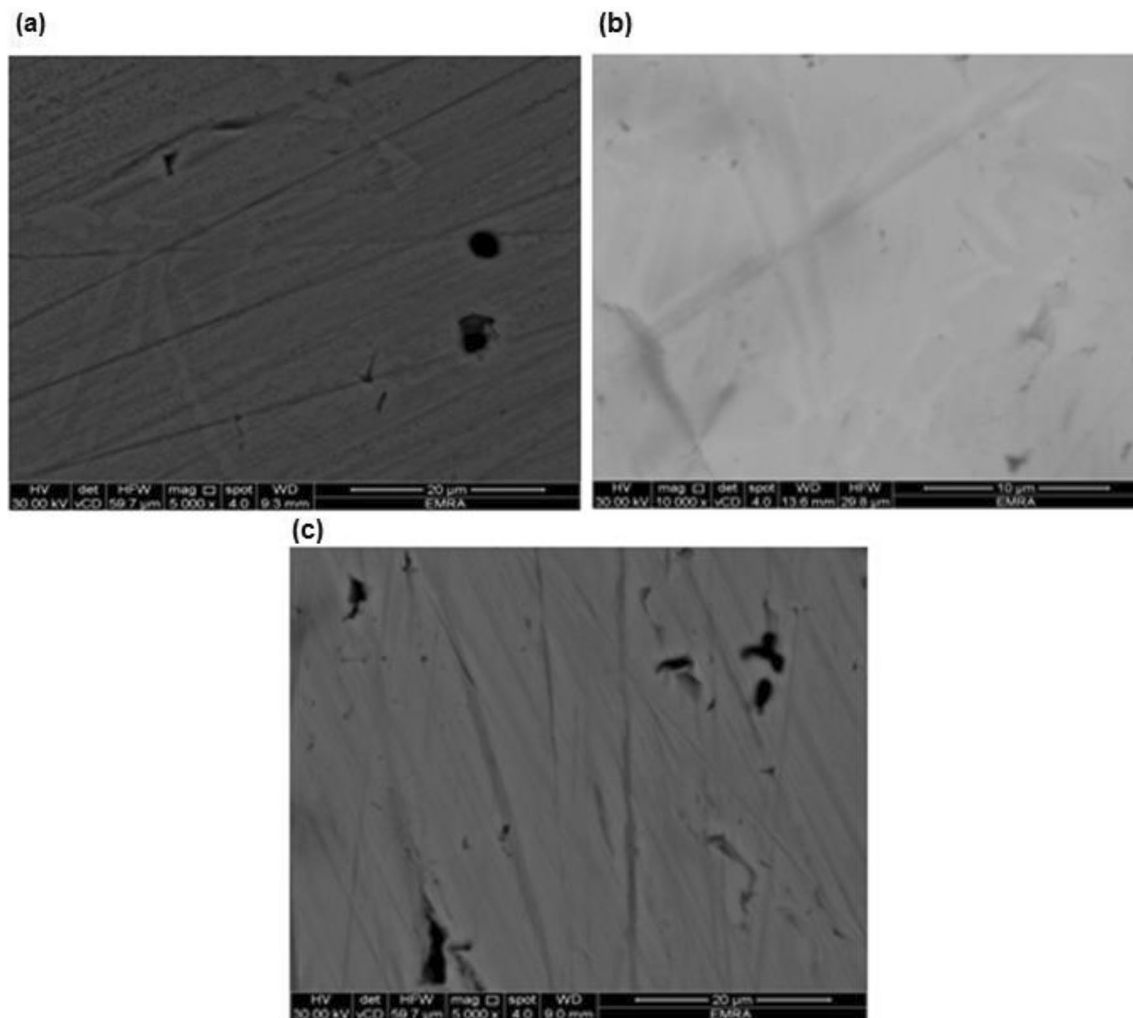| Alloy	O%
Fe	9.35
Fe–12.3Al	8.09
Fe–28.6Al	7.61
Fe–7.7Al–8.5Ti	4.44

analysed the results, designed the figures, and wrote the manuscript. MMR and GMA verified the final draft for publication.

Compliance with Ethical Standards

Conflict of interest The authors declare that they have no conflicts of interest.

Author Contributions MMR, GMA, and AHA conceived of the idea. MMR supervised the work, devised the main conceptual proof outline, and was in charge of overall direction and planning. GMA performed alloys casting and helped in almost all of the technical details. AHA prepared alloys, performed all the experiments and the measurements,

References

1. Sherif E-SM, Almajid AA, Khalil KA, Junaedi H, Latief F (2013) Electrochemical studies on the corrosion behavior of API X65 pipeline steel in chloride solutions. Int J Electrochem Sci 8:9360–9370
2. Zamanzade M, Barnoush A, Motz C (2016) A review on the properties of iron aluminide intermetallics. Crystals 6:10
3. Ruan Y, Mohajerani A, Dao M (2016) Microstructural and mechanical-property manipulation through rapid dendrite growth and undercooling in an Fe-based multinary alloy. Sci Rep 6:31684

Fig. 13 Scanning electron micrographs of Fe–Al–Ti alloy after 60 min immersion at 25 °C. **a** pH 2, **b** pH 7, **c** pH 12

4. Brotzu A, Felli F, Marra F, Pilone D, Pulci G (2018) Mechanical properties of a TiAl-based alloy at room and high temperatures. Mater Sci Technol 34:1847–1853

5. Wen Y, Wang L, Liu H, Song L (2017) Ab initio study of the elastic and mechanical properties of B19 TiAl. Crystals 7:39

6. Chanbi D, Ogam E, Amara S, Fellah Z (2018) Synthesis and mechanical characterization of binary and ternary intermetallic alloys based on Fe–Ti–Al by resonant ultrasound vibrational methods. Materials 11:746

7. Nazarova T, Imayev V, Imayev R, Fecht H-J (2017) Study of microstructure and mechanical properties of Ti–45Al–(Fe, Nb) (at.%) alloys. Intermetallics 82:26–31

8. Kutz TN, Zander D (2017) The influence of chromium on the passivation of Fe3Al iron aluminides, investigated via potentiodynamic polarization in 0.25 M H$_2$SO$_4$. Corrosion 73:648–654

9. Karapanou E, Lekatou A, Sfikas A, Georgatis E, Lentzaris K, Karantzalis A (2017) Vacuum arc melting processed Fe-Al matrix based intermetallic composites, reinforced with VC phases: assessment of microstructure, sliding wear and aqueous corrosion response. Mater Sci Eng Adv Res. https://doi.org/10.24218/msear.2017.1S

10. Rosalbino F, Carlini R, Zanicchi G, Scavino G (2016) Effect of copper alloying addition on the electrochemical corrosion behaviour of Fe3Al intermetallic in sulphuric acid solution. Mater Corros 67:1042–1048

11. Peng J, Moszner F, Rechmann J, Vogel D, Palm M, Rohwerder M (2019) Influence of Al content and pre-oxidation on the aqueous corrosion resistance of binary Fe–Al alloys in sulphuric acid. Corros Sci 149:123–132

12. Romo L, Gonzalez-Rodriguez J, Porcayo-Calderon J, Guardian R, Salinas-Bravo V (2015) A study on the effect of Co, Cr and Ti on the corrosion of FE40AL intermetallic in molten NaCl–KCl mixture. Intermetallics 67:156–165

13. Bodunrin MO, Chown LH, van der Merwe JW, Alaneme KK (2019) Corrosion behaviour of low-cost Ti–4.5 Al–x V–y Fe alloys in sodium chloride and sulphuric acid solutions. Corros Eng Sci Technol 54:637–648

14. Bodunrin MO, Chown LH, van der Merwe JW, Alaneme KK (2018) Corrosion behaviour of Ti–Al–xV–yFe experimental alloys in 3.5 wt% NaCl and 3.5 M H2SO4. Mater Corros 69:770–780

15. Bodunrin MO (2018) Hot deformation and corrosion behaviour of low-cost α + β titanium alloys with aluminium, vanadium and iron addictions. Dissertation, University of Witwatersrand, Johannesburg

16. Zhang LC, Chen LY (2019) A review on biomedical titanium alloys: recent progress and prospect. Adv Eng Mater 21:1801215

17. Lu J, Zhao Y, Niu H, Zhang Y, Du Y, Zhang W, Huo W (2016) Electrochemical corrosion behavior and elasticity properties of Ti–6Al–xFe alloys for biomedical applications. Mater Sci Eng C 62:36–44

18. Dai N, Zhang L-C, Zhang J, Chen Q, Wu M (2016) Corrosion behavior of selective laser melted Ti–6Al–4V alloy in NaCl solution. Corros Sci 102:484–489

19. Khan MM, Shabib I, Haider W (2019) A combinatorially developed Zr–Ti–Fe–Al metallic glass with outstanding corrosion resistance for implantable medical devices. Scripta Mater 162:223–229

20. Qiu Y, Thomas S, Fabijanic D, Barlow A, Fraser H, Birbilis N (2019) Microstructural evolution, electrochemical and corrosion properties of AlxCoCrFeNiTiy high entropy alloys. Mater Des 170:107698

21. Yin Y, Pan C, Zhang R, Zhao C, Qu Y (2018) The effect of Ti addition on the microstructure and properties of high chromium iron-based coatings. J Alloys Compd 765:782–790

22. Sandlöbes S, Korte-Kerzel S, Raabe D (2019) On the influence of the heat treatment on microstructure formation and mechanical properties of near-α Ti–Fe alloys. Mater Sci Eng A 748:301–312

23. Candan S, Cim S, Candan E (2019) Effectiveness of Ti microalloying for the suppression of Fe impurities in AZ91 Mg alloys and associated corrosion properties. Mater Test 61:1165–1170

24. Zhao Y, Wang M, Cui H, Zhao Y, Song X, Zeng Y, Gao X, Lu F, Wang C, Song Q (2019) Effects of Ti-to-Al ratios on the phases, microstructures, mechanical properties, and corrosion resistance of Al2–xCoCrFeNiTix high-entropy alloys. J Alloys Compd 805:585–596

25. Bolzoni L, Ruiz-Navas EM, Gordo E (2016) Understanding the properties of low-cost iron-containing powder metallurgy titanium alloys. Mater Des 110:317–323

26. Flores-Chan J, Torres-Islas A, Patiño-Carachure C, Rosas G, Espinosa-Medina M (2016) Corrosion study of Al–Fe (20 wt%) alloy in seawater alkaline solutions. Int J Electrochem Sci 11:7359–7369

27. Huape-Padilla E, Sánchez-Carrillo M, Flores-De los Ríos J, Espinosa-Medina M, Bautista-Margulis R, Ferrer-Sánchez M, Carbajal-de la Torre G, Bejar-Gómez L, Chacón-Nava J, Martinez-Villafane A (2015) Corrosion study of Fe–Al intermetallic alloys in simulated acid rain. Int J Electrochem Sci 10:2141–2154

28. Brito P, Schuller É, Silva J, Campos TR, de Araújo CR, Carneiro JR (2017) Electrochemical corrosion behaviour of (100), (110) and (111) Fe$_3$Al single crystals in sulphuric acid. Corros Sci 126:366–373

29. Masahashi N, Kimura G, Oku M, Komatsu K, Watanabe S, Hanada S (2006) Corrosion behavior of iron–aluminum alloys and its composite steel in sulfuric acid. Corros Sci 48:829–839

30. Chiang W-C, Luu W-C, Wu J-K (2006) Effect of aluminum content on the passivation behavior of Fe–Al alloys in sulfuric acid solution. J Mater Sci 41:3041–3044

31. Banovic SW, DuPont JN, Marder AR (2000) The effect of aluminum content on the corrosion behavior of Fe–Al alloys in reducing environments at 700° C. Metall Mater Trans A 31:1805–1817

32. Tomaszewicz P, Wallwork GR (1983) Observations of nodule growth during the oxidation of pure binary iron–aluminum alloys. Oxid Met 19:165–185

33. Sukiman NL, Zhou X, Birbilis N, Hughes AE, Mol JMC, Garcia SJ (2012) Thompson GE Durability and corrosion of aluminium and its alloys: overview, property space, techniques and developments. In: Ahmad Z (ed) Aluminium alloys—new trends in fabrication and applications. InTech, Rijeka, pp 47–97

34. Ghali E (2010) Corrosion resistance of aluminum and magnesium alloys: understanding, performance, and testing. Wiley, New Jersey

35. McCafferty E (2010) Thermodynamics of corrosion: pourbaix diagrams. Introduction to corrosion science, 1st edn. Springer, New York, pp 95–117

36. Macdonald DD, Real S, Smedley SI, Urquidi-Macdonald M (1988) Evaluation of alloy anodes for aluminum-air batteries IV. Electrochemical impedance analysis of pure aluminum in at 25° C. J Electrochem Soc 135:2410–2414

37. Badawy WA, Al-Kharafi FM, El-Azab AS (1999) Electrochemical behaviour and corrosion inhibition of Al, Al-6061 and Al–Cu in neutral aqueous solutions. Corros Sci 41:709–727

38. Macdonald JR (1987) Impedance spectroscopy and its use in analyzing the steady-state AC response of solid and liquid electrolytes. J Electroanal Chem Interfacial Electrochem 223:25–50

39. Hladky K, Callow LM, Dawson JL (1980) Corrosion rates from impedance measurements: an introduction. Br Corros J 15:20–25

40. Brug G, Van Den Eeden A, Sluyters-Rehbach M, Sluyters J (1984) The analysis of electrode impedances complicated by the presence of a constant phase element. J Electroanal Chem Interfacial Electrochem 176:275–295

41. Abady GM, Hilal NH, El-Rabiee M, Badawy WA (2010) Effect of Al content on the corrosion behavior of Mg–Al alloys in aqueous solutions of different pH. Electrochim Acta 55:6651–6658

42. Arzola-Peralta S, Llongueras JG, Palomar-Pardavé M, Romero-Romo M (2003) Study of the electrochemical behaviour of a carbon steel electrode in sodium sulfate aqueous solutions using electrochemical impedance spectroscopy. J Solid State Electrochem 7:283–288

43. Bhadeshia H, Honeycombe R (2017) Steels: microstructure and properties. Cambridge University Press, Cambridge

44. Saheb N, Laoui T, Daud AR, Harun M, Radiman S, Yahaya R (2001) Influence of Ti addition on wear properties of Al–Si eutectic alloys. Wear 249:656–662

45. Weng S, Huang Y, Xuan F, Luo L (2015) Correlation between microstructure, hardness and corrosion of welded joints of disc rotors. Procedia Eng 130:1761–1769

46. Jaradeh M, Tr Carlberg (2005) Effect of titanium additions on the microstructure of DC-cast aluminium alloys. Mater Sci Eng A 413:277–282